Origin of potassium promotion effects on CuCl$_2$/γ-Al$_2$O$_3$ catalyzed ethylene oxychlorination

Yanying Qi[a], Endre Fenes[a], Hongfei Ma[a], Yalan Wang[a], Kumar Ranjan Rout[a,b], Terje Fuglerud[c], Marco Piccinini[d], De Chen[a,*]

[a] Department of Chemical Engineering, Norwegian University of Science and Technology, Sem Sælands vei 4, N-7491 Trondheim, Norway
[b] SINTEF Industry, Norway
[c] INOVYN, Norway
[d] INOVYN, Rue Solvay 39-5190 Jemeppe-sur-Sambre, Belgium

ARTICLE INFO

ABSTRACT

Potassium promoters are widely used in industrial catalysts of ethylene oxychlorination to achieve optimum performance. However, the origin of the promoter effect is not fully understood. Herein, we investigated the potassium promotion effect on CuCl$_2$/γ-Al$_2$O$_3$ catalyzed ethylene oxychlorination by kinetic experiments and DFT calculations. Kinetic experiments observed the effect of KCl on individual steps, and the evolution of the reaction mechanisms with Cl/Cu ratios. Further exploration via DFT found that KCl increases the formation energy of Cl vacancy (ΔE_v) and thus inhibits the reduction activity, which is attributed to the shift-down of Bader charge of Cl. ΔE_v boosts with the decline of Cl/Cu ratios; thus, ethylene can extract Cl atoms from the surface with a Cl/Cu ratio of 2, while it anchors to metal atoms at lower Cl/Cu ratios. The distinct adsorption modes reflect the evolution of reaction mechanisms with Cl/Cu ratios. KCl facilitates the adsorption of oxygen owing to the shift-up of the Bader charge of Cu atom. Potassium reduces the Gibbs free energy barrier of the oxidation step, which agrees with the experimental observation. It is concluded that the potassium promoter effect on the catalytic performance mainly results from the modification of the charge of surface atoms.

1. Introduction

Polyvinyl chloride (PVC) is a critical synthesis plastic with a wide range of applications, and thus, its corresponding monomer, vinyl chloride (VCM), is a target synthetic platform molecule [1,2]. VCM is produced either by hydrochlorination of acetylene or 1,2-dichloroethane (EDC) thermal cracking [3–5]. EDC is derived by direct chlorination of ethylene or by ethylene oxychlorination on a CuCl$_2$ based catalyst. The latter process recycles the wasted HCl in the EDC cracking, which provides significant commercial and environmental benefits to the industry. Substantial efforts have been devoted to the ethylene oxychlorination processes [2,6–9]. It is generally accepted that the process follows a Mars and van Krevelen mechanism, where the catalyst itself partakes in the reaction. Cl vacancy on the catalyst surface is generated in the reduction step, and then oxygen inserted into the catalyst in the oxidation step, followed by a hydrochlorination step. The active sites or oxidation states of catalysts are entirely dynamic and depend on the relative reduction and oxidation rates, which complicates the investigation of the reaction mechanism.

Cupric chloride supported on a porous support such as alumina is widely applied in the industrial process owing to the high EDC selectivity. One of the main challenges is the loss of active phase via the volatilization of cuprous copper. Numerous additives such as alkaline or alkaline earth chlorides are added in the catalyst to improve the catalytic performance and stability. KCl is the most common promoter in fixed bed technologies in combination with CsCl, NaCl, or LiCl. The promotion effect of potassium was investigated by a large number of experimental work [6,7,10–16]. The formation of a copper-potassium mixed salt was proved by monitoring the Cu^{2+} d-d transitions with UV–vis spectrometer and the CO starching frequency with IR spectroscopy [15,16]. The mixture modifies the chemical nature of the active phase and inhibits the ethylene adsorption or Cl migration on the surface. Besides, it is reported that the competition adsorption between Cu^{2+} and K on the cationic vacancies at the alumina surface alters the interaction between Cu^{2+} and the support and thus increases the amount of the reducible Cu^{2+} [7]. However, the exact structure of the catalyst is still unknown. The other important observation is that the potassium shifts the rate-determining step from CuCl oxidation to CuCl$_2$

* Corresponding author.
 E-mail address: de.chen@ntnu.no (D. Chen).

reduction [6,7,15], which results in the significant increase of Cu^{2+} content. Although substantial effects from the characterization technologies and kinetic experiments, there are still unsolved questions. For example, whether the structure modification or the alteration of electronic properties induced by the potassium promoter results in the change of the rate-determining step. Therefore, a fundamental and comprehensive understanding of the potassium promoter on the nature of the active phase and the adsorption behavior of various reactants is highly desired.

In the study, reaction rates of reduction step and oxidation step for K-doped $CuCl_2$/γ-Al_2O_3 catalysts were measured by using UV–ViS-NIR spectrometer and MS. The evolution of the reaction rate with the number of active sites was detected. Then, van der Waals (vdW)-corrected DFT calculations were employed to explore the potassium promotion effect. We exploited the effect of KCl on the interface structure and the charge transfer between $(CuCl_2)_3$ and γ-Al_2O_3(1 1 0). The structures of active sites with different Cl/Cu ratios (i.e., various Cu coordination number) were constructed by removing chlorine atoms. Moreover, the promoter effect on the formation energy of Cl vacancy was explored. We also investigated the effect of KCl on the adsorption of ethylene, dioxygen, and oxygen, as well as oxidation barriers on the surfaces with different Cl/Cu ratios. Bader charge analysis was performed to rationalize the promoter effect of KCl on the adsorption of ethylene and oxygen. Besides, the Gibbs free energy barriers were analyzed.

2. Methods

2.1. Experimental methods

The catalysts were prepared by co-impregnating $CuCl_2$·$2H_2O$ and KCl on γ-Al_2O_3 according to the incipient wetness impregnation and were dried at 120 °C. The catalysts K0.23Cu0.77 contain 1.2 wt% K along with 5 wt% Cu. The catalysts were labelled according to the mole fraction of the metal. The characterization method of catalysts has been reported in the previous paper [7,17], and the physical properties are summarized below in Table 1.

The experiments were performed in a fixed-bed quartz reactor, and the scheme has already been illustrated in the previous paper [7,17]. Operando Avaspec-3648 UV–Vis-NIR spectroscopy (Avantes, Netherlands) was recorded through a fiber optic probe directed towards the catalyst bed, and the effluent gases were analyzed with a Mass spectrometry (MS) (Pfeiffer). All the experiments were carried out at differential conditions, where the reaction temperature is 230 °C, and the total pressure is 1 atm. Ethylene, oxygen, and HCl, balanced with argon, were introduced stepwise into the reactor for 20 min in the transient experiments. The partial pressures of ethylene, oxygen, and HCl for individual cycles are 0.1, 0.1, and 0.05 atm, respectively. The transient data was recorded after two complete transient cycles, where the relative Cu^{2+} concentration was estimated by the Normalized Kubelka-Munk function (NKMF). The Kubelka-Munk units were evaluated at 793 nm, referring to the d-d transition of Cu^{2+}. Reaction rates of reduction and oxidation were calculated according to the following equations, where X is the conversion, W is the weight of total Cu in the catalysts, F is the molar flow rate, and 0 means the initial value.

$$r_{reduction} = \frac{X_{C2H4}}{W/F_{C2H4,0}} \tag{1}$$

Table 1
Physical properties of the catalysts.

Catalyst	Surface area [m^2/g]	Pore volume [cm^3/g]	Pore size(nm)
γ-Al_2O_3	164	0.45	10.9
K0.23Cu0.77	151	0.40	9.20

$$r_{oxidation} = \frac{X_{O2}}{W/F_{O2,0}} \tag{2}$$

The removable Cl and the CuCl concentration at time i are calculated based on the total Cu^{2+} concentration. i = [1,2,3,….N], where N is the maximum number of data points.

$$C_{Cl,i} = 2C_{Cu^{2+},i} \tag{3}$$

$$C_{CuCl,i} = C_{Cu,total,i} - C_{Cu^{2+},i} \tag{4}$$

The calculation method of the Cu^{2+} concentration has been reported by Kumar et al. [7].

2.2. Theoretical methods

We performed DFT calculations in the Vienna ab initio simulation program (VASP) 5.3 code [18–20]. The exchange-correlation functional was described by using Bayesian error estimation functional with van der Waals correlation (BEEF-vdW) functional [21]. The projected augmented wave (PAW) method [22], combined with the plane-wave expansion at a kinetic energy cut-off of 400 eV, was adopted. A $4 \times 4 \times 1$ k-point grid was used. All calculated energies and forces were converged to within 10^{-4} eV and 0.03 eV/Å, respectively. In the XRD profiles, only the alumina surface is detected. The lack of peaks ascribed to $CuCl_2$, KCl, or any form of the mixed salt phase suggests that they are well dispersed and are in contact with the support [17]. It is also reported that the $CuCl_2$ can disperse spontaneously onto the surface of the support and form a monolayer type structure because the monolayer is a thermodynamically stable form by Xie et al. [23] The support γ-Al_2O_3 was involved in the models since the strong interaction between $CuCl_2$ and the support influent the catalytic performance, as demonstrated in the literature [24]. Thus, we built the γ-Al_2O_3 surface firstly, then adsorb $CuCl_2$ to form a monolayer structure rather than simply employ a $CuCl_2$ surface. A non-spinel bulk structure of alumina was used herein, which is proposed by Digne et al. [25,26]. The optimized lattice parameters are a = 5.593 Å, b = 8.419 Å, c = 8.082 Å and β = 90.545°, which agrees well with the literature [25,27]. γ-Al_2O_3 (1 1 0) surface, the most exposed one, is employed to represent the alumina support in this work. A (1×1) supercell with eight atomic layers was selected, and a vacuum of 15 Å is set between two periodic repeated slabs. The bottom four layers were kept frozen at their corresponding bulk positions during the optimization. Numbers of initial adsorption configurations were built based on the chemical intuition. Both vertical and parallel adsorption on different sites were explored to get the optimum one. Dimer method [28] was used to locate the transition state, and the vibrational frequencies were calculated to verify the transition states with one negative mode corresponds to the desired reaction coordinates.

The adsorption energy and activation energy are calculated as $E_{ads} = E_{A+slab} - E_A - E_{slab}$ and $E_a = E_{TS} - E_{IS}$, respectively, where E_A is the total energy of the gas phase species, E_{slab} is the total energy of the slab, E_{A+slab} is the minimum total energy of molecule adsorbed on the slab. E_{TS} is the total energy of the transition state, and E_{IS} is the total energy of the initial state. Bader charge analysis [29,30] were performed to investigate the electron transfer of the model. The difference in charge density is calculated by $\Delta \rho = \rho(moleculue + slab) - \rho(slab) - \rho(molecule)$, which is visualized by using the VESTA software[31], where $\rho(moleculue + slab)$ is the charge of the optimized structure of molecule on the surface, $\rho(slab)$ is the charge of the clean surface, and $\rho(molecule)$ is the charge of free molecules.

3. Results and discussion

3.1. Kinetic evolution of reduction and oxidation steps

Cu is cycled by Cu (II) reduction and Cu (I) oxidation in a three-step
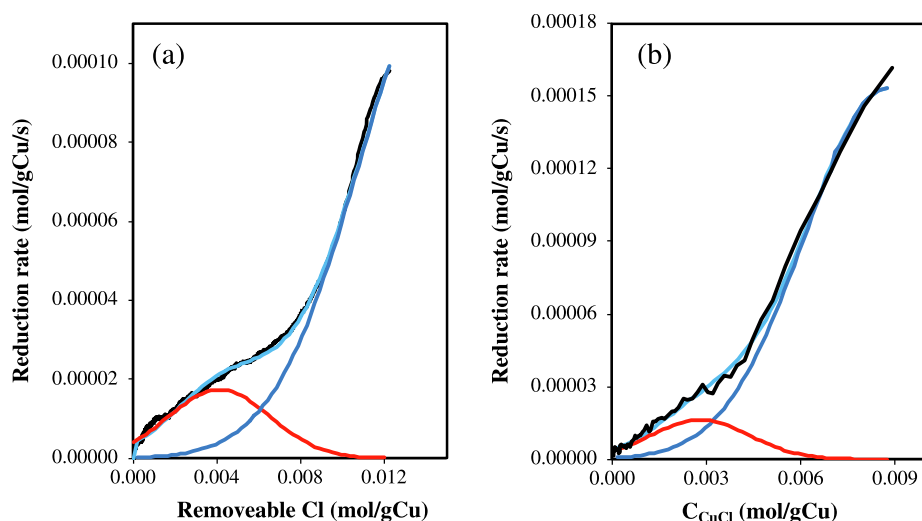
Fig. 1. (a) Reaction rate of reduction as a function of removable Cl and (b) reaction rate of oxidation as a function of the concentration of CuCl. The partial pressure of ethylene and oxygen for individual steps are 0.1 and 0.1 atm, respectively. The black lines are the experimental results, the red and dark blue curves are the simulated deconvoluted curves, and the light blue is the combination of the two deconvoluted curves. (For interpretation of the references to colour in this figure legend, the reader is referred to the web version of this article.)

reaction mechanism [8,32–34]: (1) reduction of $CuCl_2$ to CuCl, (2) oxidation of CuCl to form an oxy-chloride and (3) hydrochlorination of the oxy-chloride to $CuCl_2$. The hydrochlorination step is found to be significantly faster than the others and could be assumed kinetically irrelevant. Thus, we focus on the investigation of reduction and oxidation steps and estimate the reaction rate changes with the amount of active site for these two steps, as displayed in Fig. 1. We previously demonstrated that K-doped catalysts increased the initial turnover frequency of the oxidation reaction by 37% and reduced the initial turnover frequency of the reduction reaction by 66% compared to the neat $CuCl_2$ catalyst [17].

Fig. 1 elucidates that the reaction rate of the reduction step declines with a decrease in the concentration of removable Cl. The curve is nonlinear and can be deconvoluted into two separate curves by Gaussian deconvolution. It indicates the structure of active sites and the reaction mechanism vary with the concentration of removable Cl. Likewise, the oxidation rate can also separate into two curves correlated to the CuCl concentration. It means that the reaction mechanisms for both the reduction and oxidation steps evolve with the concentration of the active sites. The different concentrations of removable Cl and CuCl could be represented by various Cl/Cu ratios of the surface. Thus, it can be deduced that the structure of the active sites and the reaction mechanism change with the Cl/Cu ratios of the catalyst. In the following sections, we investigated ethylene adsorption and oxygen dissociation on the surfaces with different Cl/Cu ratios to rationalize the evolution of reaction mechanism and the potassium promotion effect on the individual steps.

3.2. Investigation the promoter effect by DFT calculation

The theoretical calculations were performed to exploit the origin of the potassium promotion effect on the reduction and oxidation steps compared to the neat catalyst and the evolution of the reaction mechanisms with the change of the Cl/Cu ratios.

3.2.1. K-promoted $CuCl_2$ clusters on γ-Al_2O_3 (1 1 0) surface

Firstly, the models were built to represent the neat catalyst and K-promoted catalyst. The most stable configuration of $(CuCl_2)_3$/γ-Al_2O_3 (1 1 0), corresponding to a Cu loading of 6%, is shown in Fig. 2. The structure is built by placing one $CuCl_2$ molecule on the most stable $(CuCl_2)_{n-1}$/γ-Al_2O_3 (1 1 0). In the model of $CuCl_2$/γ-Al_2O_3 (1 1 0), the average Cu-O length in our model is 1.96 Å, which agrees well with experimental results (1.94 ± 0.1 Å) detected by Lamberti et al. [35] The strong interaction results in the distortion of the $CuCl_2$ when it is adsorbed on the alumina surface, that is, the Cu−Cl bond is elongated by 0.62 Å and $\theta_{Cl-Cu-Cl}$ changes to 97° from the original 180°. We

exploited the various possibilities with different adsorption sequence of KCl and $CuCl_2$ to find the most stable configuration of (3$CuCl_2$ + KCl) cluster on γ-Al_2O_3 (1 1 0). Both the vertical and parallel adsorption of KCl and $CuCl_2$ are considered.

KCl binds strongly with the surface by the bonds of Cl-Al_A, K-O_5, and K-O_6 with the adsorption energy of −2.87 eV, where the strong adsorption is due to the high degree of coordinative unsaturation of the γ-Al_2O_3 (1 1 0) surface. The K-Cl bond is elongated by 0.6 Å. We tested two possibilities of KCl and $CuCl_2$ co-adsorption, which is adding another $CuCl_2$ on the surface with one pre-adsorbed KCl and contrariwise. $KCuCl_3$ salt is formed no matter the sequence of adding molecules. The most stable structure is formed by placing KCl on the surface with a pre-adsorbed $CuCl_2$. The adsorption energy of KCl is −2.39 eV on the surface with a pre-adsorbed $CuCl_2$, which is weaker than this on the clean surface. The newly added Cl atom binds strongly with the copper atom and squeezes away the original Cl bound to the copper atom. The second layer is generated upon the adsorption of the third $CuCl_2$ molecules. The adsorption energy of the second and third $CuCl_2$ molecule are −1.59 eV and −0.84 eV, respectively, which are smaller than these without co-adsorbed KCl. It is deduced that the competition adsorption between $CuCl_2$ and KCl on the alumina surface weakens the interaction between copper chlorides and the support (see Table 2).

Bader charge analysis was performed to study the electron transfer between the molecules and the surface (see Table 3). The first layer Cl atoms (i.e., Cl_2, Cl_3, Cl_5, and Cl_6) accept electrons from aluminum and copper atoms, while the second layer Cl atoms (i.e., Cl_1, and Cl_4) can directly extract electrons only from the copper atoms. The more negative Bader charge of first layer Cl atoms was observed, as shown in Table 3. The average Bader charge of the first layer oxygen atoms in alumina surface increases to −1.54 e from −1.61 e upon the adsorption of $(CuCl_2)_3$, which is due to the competition between Cl and O to extract the electron of Al. Cl accepts more electrons from the surface Al atoms since electronegativity of Cl is larger than O.

Similar to $(CuCl_2)_3$/γ-Al_2O_3 (1 1 0), the charge of the first layer Cl atoms (i.e., Cl_2, Cl_3, Cl_6, and Cl_7) is more negative than the second layer Cl atoms on the (3$CuCl_2$ + KCl)/γ -Al_2O_3 (1 1 0). The charge transfer between $CuCl_2$ and the alumina surface is more substantial compared to that between KCl and the alumina surface, as shown in Fig. 3b. It is found that the potassium atom donates electrons mainly to the neighboring Cl atoms rather than the surface oxygen atoms, as illustrated in Fig. 3c, which indicates the interaction between KCl and the alumina surface is weak. Thus, the average Bader charge of the first layer oxygen atoms (i.e., −1.53 e) is similar to $(CuCl_2)_3$, while the average Cl charge decreases to −0.61 e via the addition of KCl.

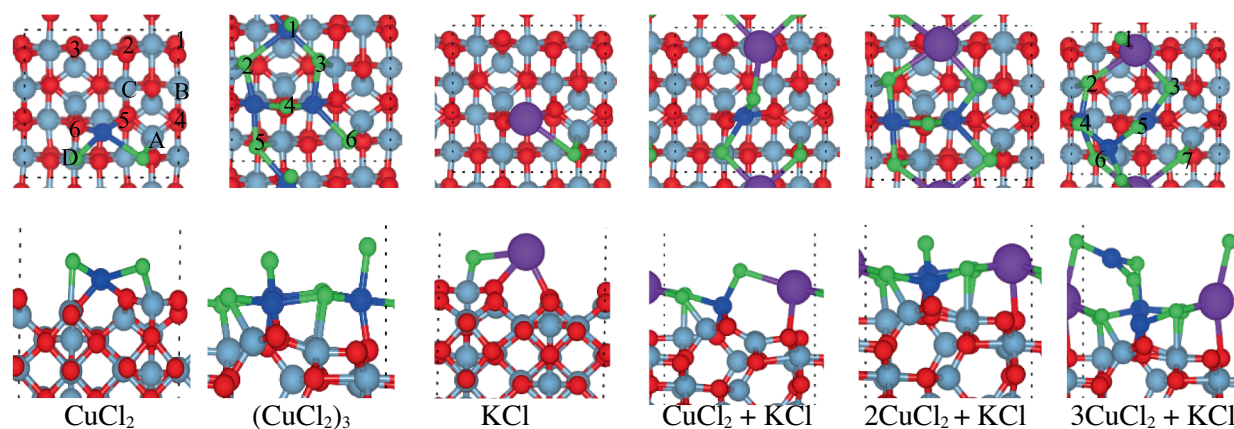**Fig. 2.** Top views (top) and side views (bottom) of the most stable configurations on the γ-Al$_2$O$_3$ (1 1 0) surface. Red balls represent O in alumina, gray balls are Al, green balls are Cl, blue balls are Cu, the purple ball is K. The same colors are employed in the whole paper. (For interpretation of the references to colour in this figure legend, the reader is referred to the web version of this article.)

3.2.2. Formation energy of Cl vacancy

As mentioned previously, Cl vacancy is formed in the reduction step, and thus we firstly examined the formation energy of Cl vacancy for copper chloride catalysts. The formation energy of oxygen vacancy has been widely used in the studies of oxides to describe the oxidizing ability, and smaller formation energy of oxygen vacancy means the catalyst is a better oxidant [36–38]. Metal oxides and metal chlorides are in the same class of catalysts, and thus the formation energy of Cl vacancy (ΔE_v) may be an essential descriptor for chlorides. The Cl vacancies or the various Cl/Cu ratios are modeled by removing Cl from the clusters. $(CuCl_2)_3$-nCl(n = 1–3) and $(3CuCl_2 + KCl)$-nCl(n = 1–3) mean eliminating n number of chlorine atoms from the surface of neat catalysts and K-promoted catalysts, and the most stable configuration is shown in Fig. 4. The formation energy of chlorine vacancy ΔE_v is defined as the energy difference between $(CuCl_2)_3$-nCl with ½ Cl$_2$ (g) and $(CuCl_2)_3$-(n-1)Cl.

The formation energy for the first Cl vacancy is in the sequence of Cl$_1 \sim$ Cl$_2 \sim$ Cl$_3$ < Cl$_5$ < Cl$_4$ < Cl$_6$ and the lowest one is 0.19 eV for $(CuCl_2)_3$/γ-Al$_2$O$_3$ (1 1 0). If Cl$_2$ or Cl$_3$ is eliminated in the initial configuration, the Cl$_1$ atom will move to the vacancy site after the optimization, which indicates that the surface Cl atom is mobile and can migrate on the surface. The electrons are re-distributed after the elimination of one chlorine atom. The charge of chlorine atoms becomes more negative, while the charge of copper atoms decreases with the elimination of Cl as displayed in Table 2. The most stable configurations of $(CuCl_2)_3 - 2Cl$ and $(CuCl_2)_3 - 3Cl$ are generated by eliminating Cl$_4$ and Cl$_2$, with the formation energies are 0.76 eV and 1.18 eV, respectively. The formation energy of the fourth Cl vacancy becomes extremely high (i.e., 3.14 eV), which indicates that removing the fourth Cl is arduous, and Cu$^+$ is stable. An isolated chlorine atom forms and the clusters become a dispersed linear shape from a polygon upon the elimination of chlorine atoms.

The first Cl vacancy is derived by removing Cl$_3$ from $(3CuCl_2 + KCl)$/γ -Al$_2$O$_3$ (1 1 0), and the formation energy of the first Cl vacancy is 0.22 eV, which is slightly enhanced compared to $(CuCl_2)_3$ (i.e., 0.19 eV). The formation energy of the first Cl vacancy is in the order of Cl$_3$ < Cl$_5$ < Cl$_6$ < Cl$_4 \sim$ Cl$_2 \sim$ Cl$_1$ < Cl$_7$. The electrons on the surface are re-assigned among various Cl atoms after the chlorine

atom is eliminated, which is similar to $(CuCl_2)_3$/γ-Al$_2$O$_3$ (1 1 0). The formation energies of the second and third Cl vacancies are 0.81 eV and 1.57 eV by eliminating Cl$_4$ and Cl$_2$, respectively. The average charge of Cu decreases with the eliminating of Cl atoms, while the charge of K keeps constant as displayed in Table 2.

The formation energy of Cl vacancy increases with the decline of Cl/Cu ratios for both the neat Cu catalyst and the potassium promoted catalyst, as shown in Fig. 5. Potassium increases the formation energy of Cl vacancy for the surfaces with a lower Cl/Cu ratio (i.e., 1.66 and 1.33). Both Cl and O atoms accept more electron from the metal atoms, and thus, their Bader charges decrease with the elimination of Cl atoms. The lower Cl charge reflects the stronger interaction between Cl and other atoms, and therefore, the reduction of the Cl charge results in the increment of the formation energy of Cl vacancy. The curves varied for neat Cu and K-promoted clusters. Compared to the copper chloride surface, the Bader charge of Cu and oxygen decreases more while the charge of Cl reduces less upon the elimination of three Cl atoms from the K-promoted surface as elucidated in Table 2. It indicates that the copper atoms donate more electrons to O rather than Cl, while K transfers more electrons to the neighboring Cl, as we found via the analysis of the charge density difference in Fig. 3. The competition between K and Cu results in a more complicated electron transfer among all the atoms.

3.2.3. Promoter effect on ethylene adsorption

Ethylene adsorption on the surfaces with different Cl/Cu ratios were investigated to understand the potassium promoter effect on the reduction step. The most stable configurations are summarized in Fig. 6. Ethylene can bind with Cu on the neat $(CuCl_2)_3$ surface with a Cl/Cu ratio of 2, but in the most stable configuration with the lowest energy, it extracts two chlorine atoms to form EDC automatically. The automatic formation of EDC indicates that the reduction barrier is low, which is consistent with the experimental observation of the fast reduction rate [7,17]. Ethylene could adsorb on Cu at lower Cl/Cu ratios since the chlorine vacancy is constructed. The distinct adsorption modes of ethylene on the surfaces with various Cu/Cl ratios are attributed to the Cl/Cu ratio-dependent formation energy of Cl vacancy, as shown in Fig. 5. ΔE_v is small on the cluster with a Cl/Cu ratio of 2, which means

Table 2
The adsorption energy of different molecules.

Molecules	CuCl$_2$	KCl	CuCl$_2$ + KCl	CuCl$_2$ + KCl + CuCl$_2$	2CuCl$_2$ + KCl + CuCl$_2$
E$_{ads}$(eV)	− 2.92	− 2.87	− 2.39	− 1.59	− 0.84

Note: the adsorption energy is for the last molecule on the surface.

Table 3
A summary of the Bader charge of the surface atoms.

	Cl_1	Cl_2	Cl_3	Cl_4	Cl_5	Cl_6	Cl_7	Cl average	Cu average	K	O average	Al average
$(3CuCl_2 + KCl)$	−0.55	−0.63	−0.68	−0.46	−0.50	−0.68	−0.77	−0.61	0.90	0.87	−1.53	2.45
$(3CuCl_2 + KCl)$-Cl	−0.60	−0.63		−0.48	−0.54	−0.71	−0.80	−0.63	0.82	0.88	−1.57	2.45
$(3CuCl_2 + KCl)$-2Cl	−0.61	−0.64			−0.54	−0.68	−0.82	−0.66	0.69	0.88	−1.58	2.45
$(3CuCl_2 + KCl)$-3Cl	−0.65				−0.58	−0.71	−0.81	−0.69	0.56	0.88	−1.59	2.44
$(CuCl_2)_3$	−0.44	−0.61	−0.52	−0.43	−0.57	−0.76		−0.55	0.90		−1.54	2.45
$(CuCl_2)_3$-Cl		−0.58	−0.59	−0.47	−0.62	−0.79		−0.61	0.85		−1.56	2.45
$(CuCl_2)_3$-2Cl		−0.62	−0.49		−0.69	−0.81		−0.65	0.73		−1.56	2.45
$(CuCl_2)_3$-3Cl			−0.52		−0.71	−0.81		−0.68	0.58		−1.57	2.45

Cl atoms are easier to be extracted. ΔE_v increases with the decrease of the Cl/Cu ratio, and thus, Cl atoms become difficult to be eliminated. The adsorption energy of ethylene declines from −0.32 eV to −0.97 eV with the decrease of the Cl/Cu ratio, which is attributed to the decline in the average charge of Cu on the surface, as shown in Fig. 7. The smaller the Cu charge means that the copper atom holds a stronger capacity to donate the electron to ethylene, which results in the stronger bonding between ethylene and the copper atom.

The carbon atoms in ethylene are bound to the chlorine atom upon the adsorption of ethylene on $(3CuCl_2 + KCl)/\gamma$-Al_2O_3 (1 1 0). However, the chlorine atoms are still attached to the surface copper and potassium atoms, which are different from $(CuCl_2)_3/\gamma$-Al_2O_3 (1 1 0). It is attributed to the stronger interaction between the chlorine atoms and the other atoms on the surface with the presence of KCl, which can be reflected by the decrease of Cl charge on the surface with potassium as elucidated in Table 2. The barrier of ethylene chlorination on $3CuCl_2 + KCl/\gamma$-Al_2O_3 (1 1 0) is assumed to equal the desorption energy of EDC, which is 0.31 eV. Similar to $(CuCl_2)_3/\gamma$-Al_2O_3 (1 1 0), ethylene could bind with the metal atom when there is an available Cl vacancy. Ethylene binding with the potassium atom (i.e., −0.38 eV) and the copper atom (i.e., −0.31 eV) show similar adsorption energy on the potassium promoted surface with one Cl vacancy, which results from the fact that the first eliminated chlorine atom binds with both the potassium and copper atoms. Copper is the preferred adsorption site with an adsorption energy of −0.53 eV for ethylene adsorbed on the surface with two Cl vacancies, which may arise from the fact that the second removed Cl binding with only copper atoms. The favorite adsorption site strongly depends on the position of the in-situ generated Cl vacancy. The increase of the adsorption strength with the decrease of Cl/Cu ratios is due to the shift-down of Cu charge, which is the same as the undoped catalyst, as elucidated in Fig. 7b. Besides, a linear relationship between the adsorption energy of ethylene and the formation energy of Cl vacancy is observed in Fig. 7c, which indicating ΔE_v could be a descriptor for the oxidizing ability of the catalyst.

3.2.4. Promoter effect on oxygen dissociation

The adsorption of dioxygen and oxygen on the surfaces with different Cl/Cu ratios were examined for both undoped and K-doped catalysts. Dioxygen physically adsorbs on the $(CuCl_2)_3/\gamma$-Al_2O_3 (1 1 0) surface with a Cl/Cu ratio of 1.67, while it could bind to the surface copper atom at the Cl/Cu ratio of 1.33 and 1, where each oxygen binds with one copper atom (see Fig. 8). The adsorption energies are −0.14 eV and −0.51 eV, and the O−O bond is elongated via 0.05 Å and 0.12 Å upon the adsorption on the $(CuCl_2)_3/\gamma$-Al_2O_3 (1 1 0) surfaces with Cl/Cu ratios of 1.33 and 1, respectively. O_2 physically adsorbs on the promoted catalyst surface with Cl/Cu ratios of 1.67 and 1.33 since both the surfaces do not have two neighboring Cl vacancies. O_2 binds to copper atoms on the surface with Cl/Cu ratios of 1, and the adsorption energy is −0.57 eV. The dioxygen adsorption becomes stronger with the decline of the Cl/Cu ratio.

Atomic oxygen adsorbs on the top of a copper atom on $((CuCl_2)_3$-Cl$)/\gamma$-Al_2O_3 (1 1 0) with the adsorption energy of −1.85 eV(see Fig. 9). The adsorption mode of oxygen atom is different from dioxygen on the surface with a Cl/Cu ratio of 1.67 since one oxygen atom only needs one Cl vacancy. It sits on a bridge site of two copper atoms on $(CuCl_2)_3/\gamma$-Al_2O_3 (1 1 0) surfaces with Cl/Cu ratios of 1.33 and 1, and the adsorption energies are −2.97 eV and −3.20 eV, respectively. Oxygen atom binds with Cu or K atom for $((3CuCl_2 + KCl)$-nCl$)/\gamma$-Al_2O_3 (1 1 0). The adsorption energies are −2.54 eV, −3.60 eV, and −3.20 eV, respectively, for the K-doped surface with Cl/Cu ratios of 1.67, 1.33, and 1. The adsorption energy becomes stronger with the decrease of the Cl/Cu ratio on both undoped and K-doped catalysts, which can be explained by the shift-down of the charge of Cu, as elucidated in Fig. 10. The deviation from the linear relationship between the adsorption energy of O and the charge of Cu on the surfaces with K is due to the different adsorption structures, for example, O binds with K and Cu on the surface with a Cl/Cu of 1.66, while O only attaches to Cu on other surfaces. The lower Bader charge of Cu indicates that Cu holds a stronger ability to accept electrons and thus could more firmly bind with oxygen. The adsorption of the oxygen atom on the K-doped surface is stronger compared to the undoped surface with the same Cl/Cu ratio, which could attribute to the shift-down of Cu charge via the addition of KCl.

Besides, the relationship between the adsorption energy of oxygen on $((CuCl_2)_3$-nCl$)$ clusters and the formation energy of the nth Cl vacancy features a linear line, as illustrated in Fig. 10(c). The stronger oxygen adsorption can result in the lower barrier of dioxygen dissociation. The larger formation energy of the nth vacancy owns stronger adsorption of oxygen, and thus, it is easy to be re-oxidized, which indicates that the formation energy of Cl vacancy can also be a descriptor

(a) $(CuCl_2)_3$ and alumina　　　(b) $(3CuCl_2+KCl)$ and alumina　　　(c) KCl and neighbouring atoms
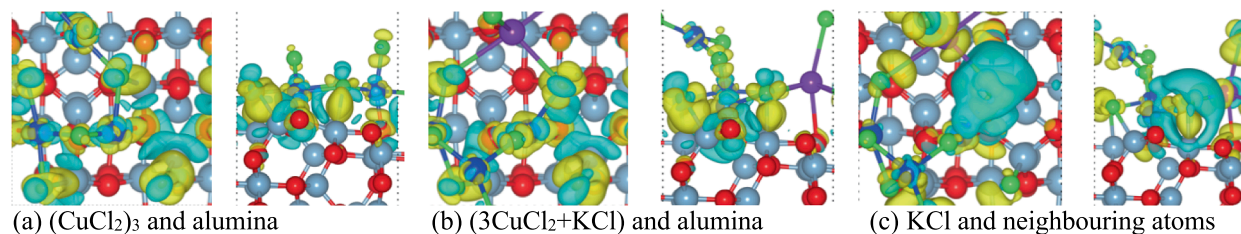
Fig. 3. Top views and side views of the charge differences in $(CuCl_2)_3/\gamma$-Al_2O_3 (1 1 0) and $(3CuCl_2 + KCl)/\gamma$-Al_2O_3 (1 1 0). The yellow and blue represent the charge accumulation and depletion isosurfaces, respectively. (For interpretation of the references to colour in this figure legend, the reader is referred to the web version of this article.)
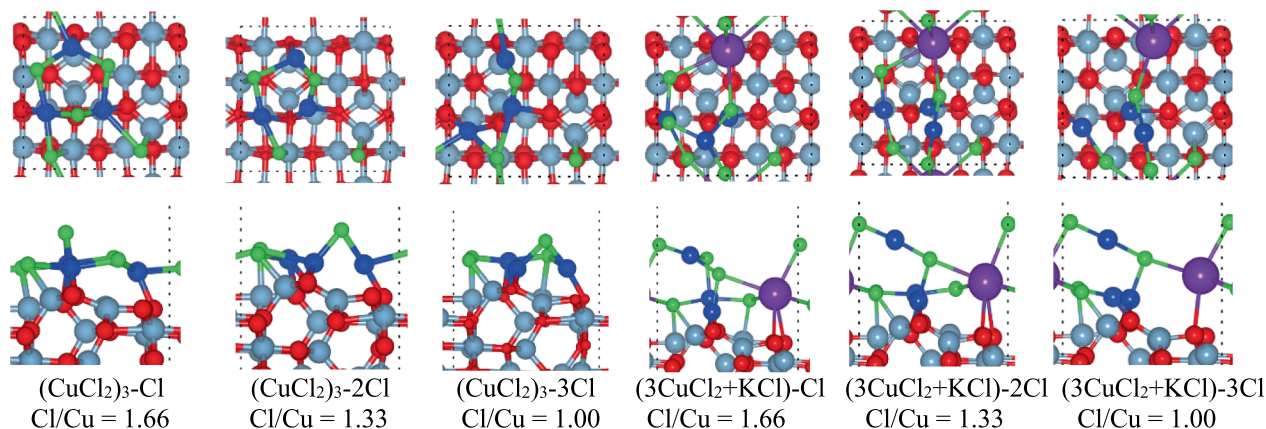
Fig. 4. Top views and side views of $(CuCl_2)_3$-nCl and $(3CuCl_2 + KCl)$-nCl. n changes from 1 to 3.

of the reducing ability of the catalyst. A smaller ΔE_v can get a catalyst with higher oxidizing ability, while a larger ΔE_v indicates a higher reducing ability of the catalyst. It suggests the catalyst to follow 'a medium principle' to complete the redox cycle, that is, modifying the surface to get a moderate ΔE_v.[33]

Moreover, we exploited the transition state of oxygen dissociation on the unpromoted surfaces and the K-promoted surfaces(see Fig. 11). Oxygen atoms sit on the Cl vacancies and bind with two cobalt atoms in the transition states on the unpromoted surfaces. The activation barriers are 1.70 eV and 0.87 eV for the $(CuCl_2)_3/\gamma$-$Al_2O_3(1\,1\,0)$ with Cl/Cu ratios of 1.33 and 1, respectively. The structure of the transition states is close to the product, which means they are late transition states. The stronger adsorption of oxygen at a low Cl/Cu ratio results in a lower barrier. The barrier increases with the increment of Cl/Cu, which is consistent with the experimental observation of the decrease of oxidation rate at lower CuCl concentration. The addition of KCl on the surface decreases the barriers to 1.68 eV and 0.51 eV for Cl/Cu ratios of 1.33 and 1, respectively. One oxygen is bound to two copper atoms, while the other one binds with two copper atoms and one potassium atom, where the bond length of K-O is 3.59 Å and 2.39 Å on the K-doped catalyst with Cl/Cu ratios of 1.33 and 1, respectively. It indicates that the structure of the transition state depends on the number of Cl vacancies (i.e., Cl/Cu ratios). Oxygen is more tightly bound to K on the K-doped surface with Cl/Cu ratios of 1, which results in a more significant decrease of the barrier via 0.36 eV.

3.3. Analysis of Gibbs free energy barrier

Gas-phase species ethylene and oxygen anchored to the solid surface in the reaction, which results in tremendous entropy lose. Thus, it is essential to explore the effects of potassium on the kinetics by comparing the Gibbs free energy barrier of the different steps. The Gibbs free energy barrier by using the following equation. The Gibbs free energy barrier is the free energy difference between the transition state (G_{TS}) and the initial state(G_{IS}).

$$G_a = G_{TS} - G_{IS} \qquad (5)$$

The Gibbs free energy of each specie was calculated by using the following equation at a temperature of 500 K.

$$G = E + E_{ZPE} + \Delta H^o(0 \rightarrow T) - TS \qquad (6)$$

where E refers to electric energy determined by DFT, E_{ZPE} is zero-point energy. H, S, and T are enthalpy, entropy, and temperature, respectively. The precise method for the calculation of zero-point energy, entropy, and enthalpy has been reported in the literature [39,40]. The Gibbs free energy of reduction step is calculated based on the results on the surface with a Cl/Cu ratio of 2, while that of oxidation step is calculated on the surface with a Cl/Cu of 1 to obtain the initial reaction rates of reduction and oxidation. The potassium dopant increases the barrier of reduction via 0.34 eV and decreases the barrier of oxidation via 0.39 eV, which agrees with the experimental observation of the potassium promotion effect(see Fig. 12) [17].
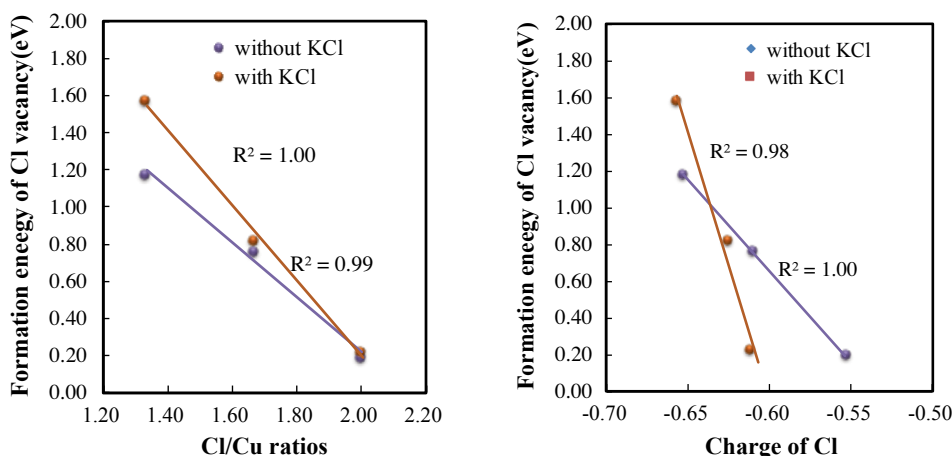

Fig. 5. The formation energy of Cl vacancy changes with Cl/Cu ratios (left), and the relationship between the formation energy of Cl vacancy and the charge of Cl (right). Note: the chlorine atom from KCl molecule is not considered in the calculation of the Cl/Cu ratio for the promoted catalyst.
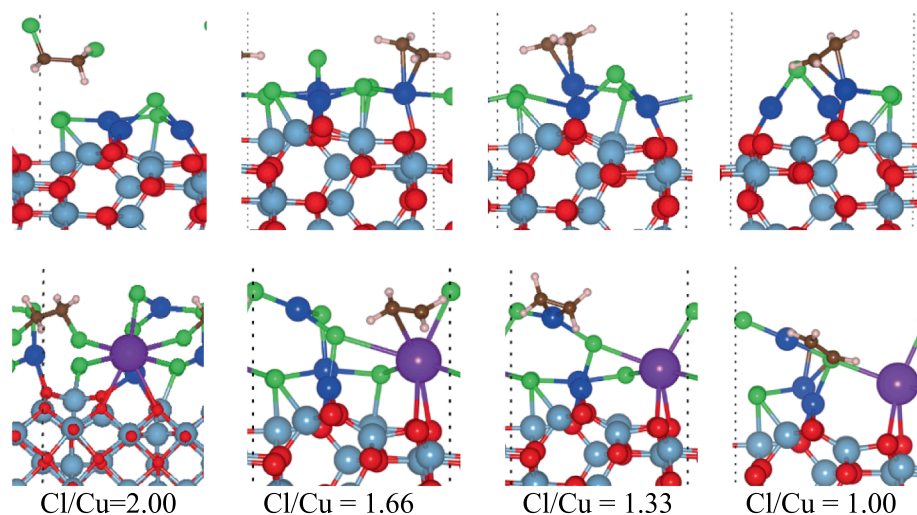
Fig. 6. Side views of ethylene adsorbed on the surfaces with various Cl/Cu ratios. The first line is for $(CuCl_2)_3/\gamma$-Al_2O_3 (1 1 0) surface, and the second is $(3CuCl_2 + KCl)/\gamma$-Al_2O_3 (1 1 0) surface.
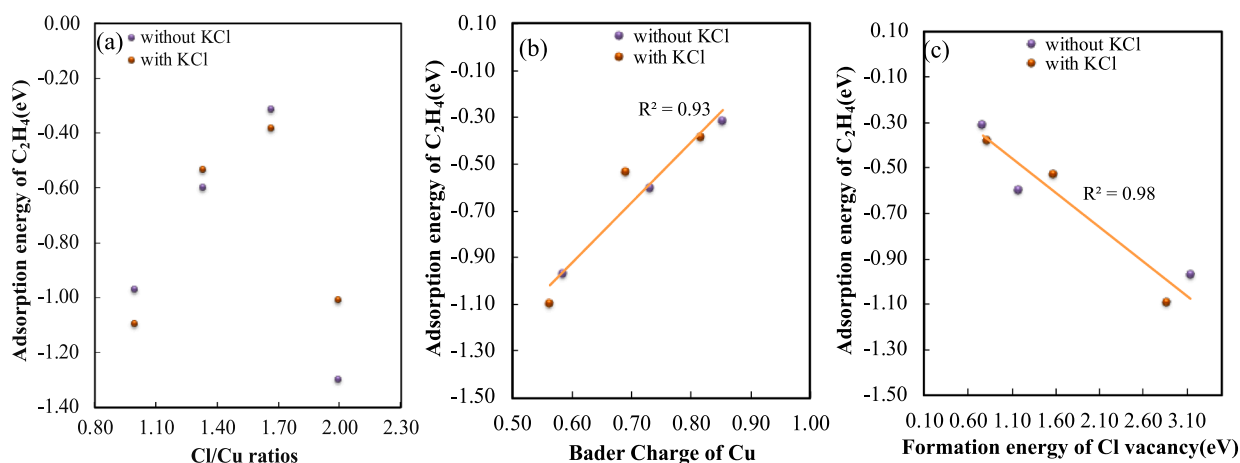

Fig. 7. (a) The adsorption energies of C_2H_4 on the surfaces with different Cl/Cu ratios, and the relationship between the adsorption energy of C_2H_4 and the charge of Cu (b) or the formation energy of Cl vacancy(c).

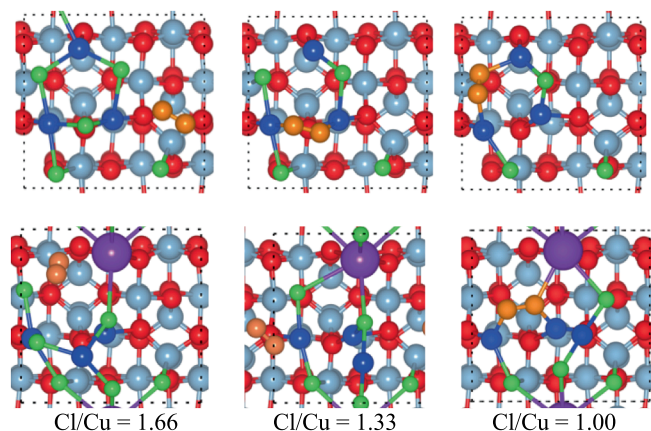**Fig. 8.** The configurations of oxygen gas adsorbed on the surfaces with different Cl/Cu ratios. The first line is for $(CuCl_2)_3/\gamma$-Al_2O_3 (1 1 0) surfaces, and the second is $(3CuCl_2 + KCl)/\gamma$-Al_2O_3 (1 1 0) surfaces.

4. Conclusion

Kinetic experiments demonstrated that the evolution of the reaction mechanism with Cl/Cu ratios on the catalyst surface. DFT calculations found that the addition of KCl distorted the original interface structure and reduced the interaction between copper chloride and the support. A salt mixture of Cu_3KCl_7 forms. Charge density difference analysis elucidates that the electron transfer between K and neighboring Cl atoms results in substantial electron accumulation around the chlorine atom, and the decline of Bader charge of Cl. Thus, it raised the formation energy of Cl vacancy upon the addition of KCl. The formation energy of Cl vacancies increases with the decrease of Cl/Cu ratios on both unprompted and K-promoted catalyst surfaces, which attributes to the decline in the Cl charge at lower Cl/Cu ratios.

Two distinct adsorption modes of ethylene were detected for the K-promoted catalyst. Ethylene binds with two chlorine atom on the surface with a Cl/Cu ratio of 2, while it is bound to copper or potassium atom on the surface with lower Cl/Cu ratios. The adsorption site at lower Cl/Cu ratios depends on the position of Cl vacancy. A linear relationship between the adsorption energy of ethylene on the surface with lower Cl/Cu ratios and the Bader charge of copper atoms are suggested. Moreover, it is found that the adsorption strength of oxygen
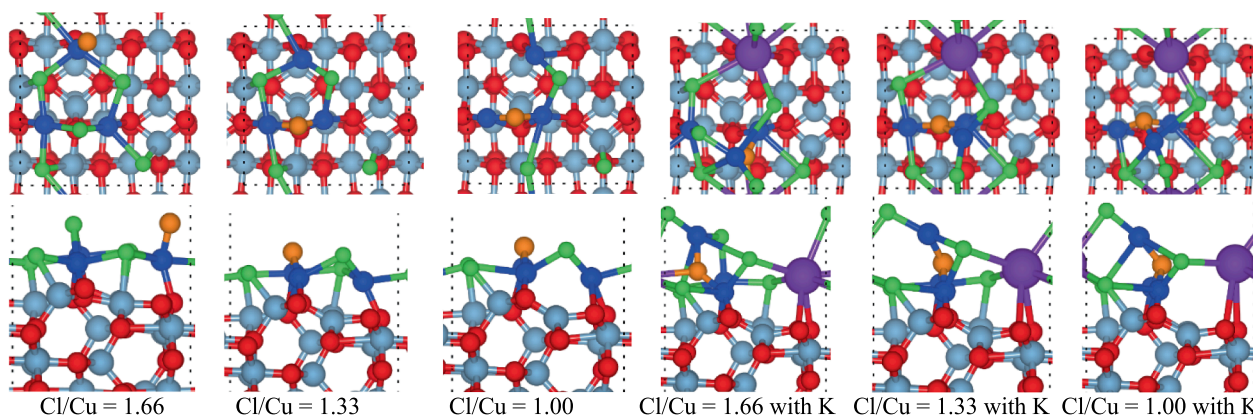
Fig. 9. The configurations of oxygen adsorbed on the surfaces with different Cl/Cu ratios. The first line is for $(CuCl_2)_3/\gamma$-Al_2O_3 (1 1 0) surfaces, and the second is $(3CuCl_2 + KCl)/\gamma$-Al_2O_3 (1 1 0) surfaces.
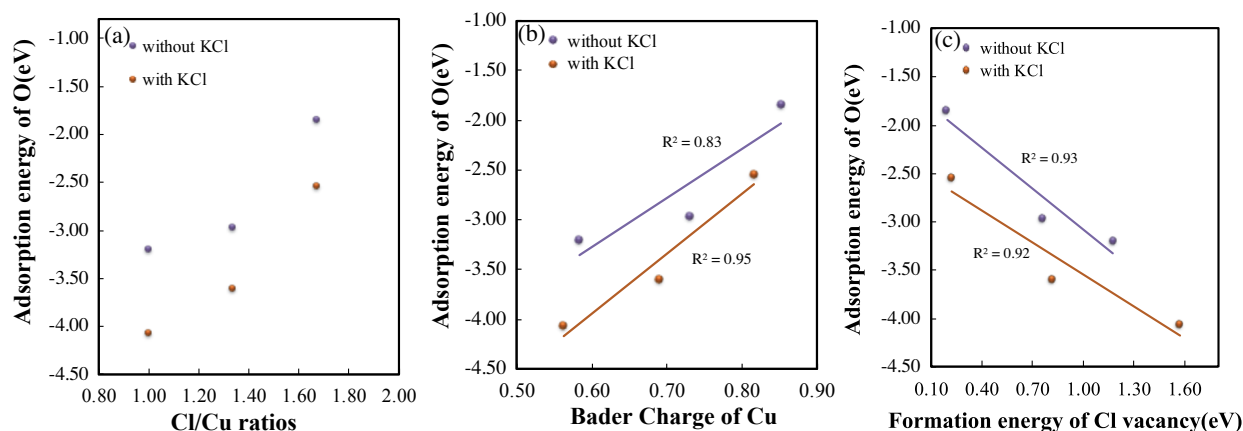

Fig. 10. (a) Adsorption energy of oxygen on the surfaces with various Cl/Cu ratios, and the relationship between the adsorption energy of O and the Bader charge of Cu(b) or formation energy of Cl vacancy(c).
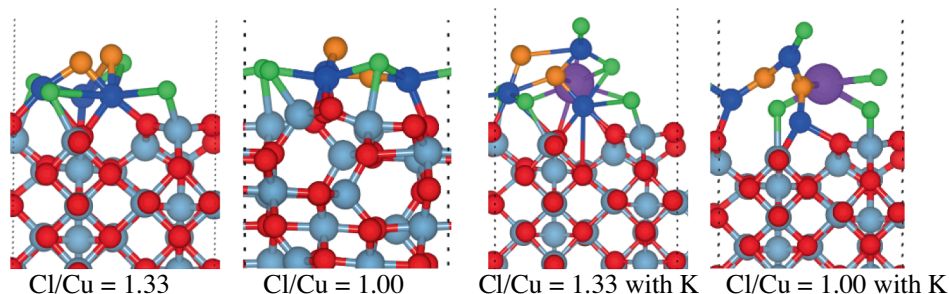

Fig. 11. The configurations of transition states of oxygen dissociation on the surfaces. Yellow balls are dissociated O. (For interpretation of the references to colour in this figure legend, the reader is referred to the web version of this article.)

enhances with the decrease of Cl/Cu ratios, which could be explained by the decline of Cu charge. Co-adsorbed KCl enhances the adsorption of oxygen and reduces the barrier of oxygen dissociation by 0.36 eV on the surface with Cl/Cu of 1 compared to the un-promoted surface.

The formation energy of Cl vacancy, resulting in the distinct adsorption modes of ethylene and the different adsorption energy of oxygen, could be a descriptor for the redox ability of the catalyst. The increase of the formation energy of Cl via KCl is attributed to the shift-down of Cl charge. The changes of adsorption energy of ethylene and oxygen on the surfaces with various Cl/Cu ratios are due to the modification of the Bader charge of Cu. Thus, the alteration of the Bader charge of surface atoms via KCl is the primary origin of the effect of KCl on catalytic performance. The findings may shed new light on the development of catalysts in ethylene oxychlorination.

CRediT authorship contribution statement

Yanying Qi: Data curation, Investigation, Methodology, Formal analysis, Writing-original draft, Writing-review & editing. **Endre Fenes:** Writing-Review & editing. **Hongfei Ma:** Writing-Review & editing. **Yalan Wang:** Writing-Review & editing. **Kumar Ranjan Rout:** Project administration. **Terje Fuglerud:** Writing-Review & editing. **Marco Piccinini:** Writing-Review & editing. **De Chen:** Funding acquisition, Writing - review & editing, Supervision.

Declaration of Competing Interest

The authors declare that they have no known competing financial interests or personal relationships that could have appeared to
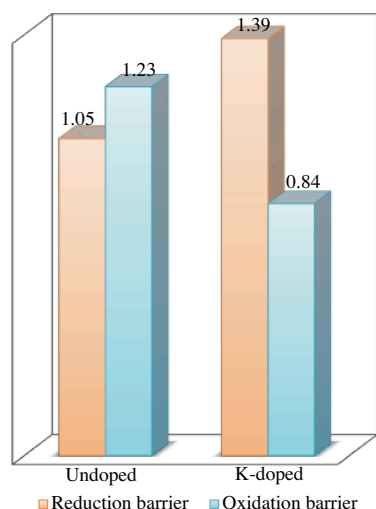
Fig. 12. The Gibbs free energy barrier of the initial reduction and oxidation steps on undoped catalysts and K-doped catalysts, where the reduction step is calculated on the surfaces with a Cl/Cu ratio of 2, and the oxidation step on the surfaces with a Cl/Cu ratio of 1.

influence the work reported in this paper.

Acknowledgments

References

[1] M. Scharfe, M. Capdevila-Cortada, V.A. Kondratenko, E.V. Kondratenko, S. Colussi, A. Trovarelli, N. López, J. Pérez-Ramírez, Mechanism of ethylene oxychlorination on ceria, ACS Catal. 8 (2018) 2651–2663.

[2] Z. Vajglová, R. Hemery, N. Kumar, K. Eränen, M. Peurla, J. Peltonen, J. Wärnå, J. Pérez-Ramírez, D.Y. Murzin, T. Salmi, Kinetics of ceria-catalysed ethene oxychlorination, J. Catal. 372 (2019) 287–298.

[3] J. Zhang, N. Liu, W. Li, B. Dai, Progress on cleaner production of vinyl chloride monomers over non-mercury catalysts, Front. Chem. Sci. Eng. 5 (2011) 514–520.

[4] K. Zhou, J. Jia, X. Li, X. Pang, C. Li, J. Zhou, G. Luo, F. Wei, Continuous vinyl chloride monomer production by acetylene hydrochlorination on Hg-free bismuth catalyst: From lab-scale catalyst characterization, catalytic evaluation to a pilot-scale trial by circulating regeneration in coupled fluidized beds, Fuel. Process. Technol. 108 (2013) 12–18.

[5] M. Scharfe, P.A. Lira-Parada, V. Paunović, M. Moser, A.P. Amrute, J. Pérez-Ramírez, Oxychlorination-dehydrochlorination chemistry on bifunctional ceria catalysts for intensified vinyl chloride production, Angew. Chem. Ger. Edit. 128 (2016) 3120–3124.

[6] C. Lamberti, C. Prestipino, F. Bonino, L. Capello, S. Bordiga, G. Spoto, A. Zecchina, S. Diaz Moreno, B. Cremaschi, M. Garilli, A. Marsella, D. Carmello, S. Vidotto, G. Leofanti, The chemistry of the oxychlorination catalyst: an in situ, time-resolved XANES Study, Angew. Chem. Int. Edit. 41 (2002) 2341–2344.

[7] K.R. Rout, M.F. Baidoo, E. Fenes, J. Zhu, T. Fuglerud, D. Chen, Understanding of potassium promoter effects on oxychlorination of ethylene by operando spatial-time resolved UV–vis–NIR spectrometry, J. Catal. 352 (2017) 218–228.

[8] K.R. Rout, E. Fenes, M.F. Baidoo, R. Abdollahi, T. Fuglerud, D. Chen, Highly active and stable CeO₂-promoted CuCl₂/Al₂O₃ oxychlorination catalysts developed by rational design using a rate diagram of the catalytic cycle, ACS Catal. 6 (2016) 7030–7039.

[9] Z. Vajglová, N. Kumar, K. Eränen, M. Peurla, D.Y. Murzin, T. Salmi, Ethene oxychlorination over CuCl2/γ-Al2O3 catalyst in micro- and millistructured reactors, J. Catal. 364 (2018) 334–344.

[10] P.S.S. Prasad, P.K. Rao, Low temperature ethylene chemisorption (L.T.E.C.): a novel technique for the characterisation of CuCl₂-KCl/[gamma]-Al₂O₃ oxychlorination catalysts, J. Chem. Soc. Chem. Comm. (1987) 951–953.

[11] A. Arcoya, A. Cortes, X.L. Seoane, Optimization of copper chloride based catalysts

[12] K. Zurowski, The mechanism of the ethene oxychlorination process when CuCl2, KCl-support catalyst is used, Pol. J. Chem. 69 (1995) 1718–1728.

[13] M. Repelewicz, Activity of cupric chloride-potassium chloride-carrier catalysts in oxidation and oxychlorination of ethylene, Pol. J. Appl. Chem. 36 (1992) 177–182.

[14] J. Liu, L. Xueju, G. Zhou, K. Zhen, W. Zhang, T. Cheng, Effect of kcl on cucl2/γ-al2o3 catalyst for oxychlorination of ethane, React. Kinet. Catal. L. 88 (2006) 315–324.

[15] N.B. Muddada, U. Olsbye, L. Caccialupi, F. Cavani, G. Leofanti, D. Gianolio, S. Bordiga, C. Lamberti, Influence of additives in defining the active phase of the ethylene oxychlorination catalyst, Phys. Chem. Chem. Phys. 12 (2010) 5605–5618.

[16] D. Gianolio, N.B. Muddada, U. Olsbye, C. Lamberti, Doped-CuCl₂/Al₂O₃ catalysts for ethylene oxychlorination: Influence of additives on the nature of active phase and reducibility, Nucl. Instrum. Methods. Phys. Res. B 284 (2012) 53–57.

[17] M.F. Baidoo, E. Fenes, K.R. Rout, T. Fuglerud, D. Chen, On the effects of K and La co-promotion on CuCl₂/γ-Al₂O₃ catalysts for the oxychlorination of ethylene, Catal. Today 299 (2018) 164–171.

[18] G. Kresse, J. Furthmuller, Efficiency of ab-initio total energy calculations for metals and semiconductors using a plane-wave basis set, Comput. Mater. Sci. 6 (1996) 15–50.

[19] G. Kresse, J. Hafner, Ab initio molecular dynamics for liquid metals, Phys. Rev. B. 47 (1993) 558–561.

[20] G. Kresse, J. Hafner, Ab initio molecular dynamics for open-shell transition metals, Phys. Rev. B. 48 (1993) 13115–13118.

[21] J. Wellendorff, K.T. Lundgaard, A. Mogelhoj, V. Petzold, D.D. Landis, J.K. Norskov, T. Bligaard, K.W. Jacobsen, Density functionals for surface science: Exchange-correlation model development with Bayesian error estimation, Phys. Rev. B. 85 (2012).

[22] G. Kresse, D. Joubert, From ultrasoft pseudopotentials to the projector augmented-wave method, Phys. Rev. B. 59 (1999) 1758–1775.

[23] Y.-C. Xie, Y.-Q. Tang, Spontaneous monolayer dispersion of oxides and salts onto surfaces of supports: applications to heterogeneous catalysis, in: D.D. Eley, H. Pines, P.B. Weisz (Eds.), Advances in Catalysis, Academic Press, 1990, pp. 1–43.

[24] Z. Vajglová, N. Kumar, K. Eränen, A. Tokarev, M. Peurla, J. Peltonen, D.Y. Murzin, T. Salmi, Influence of the support of copper catalysts on activity and 1,2-dichloroethane selectivity in ethylene oxychlorination, App. Catal. A. Gen. 556 (2018) 41–51.

[25] M. Digne, P. Sautet, P. Raybaud, P. Euzen, H. Toulhoat, Use of DFT to achieve a rational understanding of acid–basic properties of γ-alumina surfaces, J. Catal. 226 (2004) 54–68.

[26] M. Digne, P. Sautet, P. Raybaud, P. Euzen, H. Toulhoat, Hydroxyl groups on γ-alumina surfaces: a DFT study, J. Catal. 211 (2002) 1–5.

[27] D. Mei, Q. Ge, J.H. Kwak, D.H. Kim, J. Szanyi, C.H.F. Peden, Adsorption and formation of BaO overlayers on γ-Al₂O₃ surfaces, J. Phys. Chem. C 112 (2008) 18050–18060.

[28] G. Henkelman, H. Jónsson, Improved tangent estimate in the nudged elastic band method for finding minimum energy paths and saddle points, J. Chem. Phys. 113 (2000) 9978–9985.

[29] G. Henkelman, A. Arnaldsson, H. Jónsson, A fast and robust algorithm for Bader decomposition of charge density, Comp. Mater. Sci. 36 (2006) 354–360.

[30] M. Yu, D.R. Trinkle, Accurate and efficient algorithm for Bader charge integration, J. Chem. Phys. 134 (2011) 064111.

[31] K. Momma, F. Izumi, VESTA 3 for three-dimensional visualization of crystal, volumetric and morphology data, J. Appl. Crystallogr. 44 (2011) 1272–1276.

[32] G. Leofanti, A. Marsella, B. Cremaschi, M. Garilli, A. Zecchina, G. Spoto, S. Bordiga, P. Fisicaro, C. Prestipino, F. Villain, C. Lamberti, Alumina-supported copper chloride: 4. Effect of exposure to O₂ and HCl, J. Catal. 205 (2002) 375–381.

[33] G. Leofanti, A. Marsella, B. Cremaschi, M. Garilli, A. Zecchina, G. Spoto, S. Bordiga, P. Fisicaro, G. Berlier, C. Prestipino, G. Casali, C. Lamberti, Alumina-supported copper chloride 3. Effect of exposure to ethylene, J. Catal. 202 (2001) 279–295.

[34] E. Finocchio, N. Rossi, G. Busca, M. Padovan, G. Leofanti, B. Cremaschi, A. Marsella, D. Carmello, Characterization and catalytic activity of CuCl₂-Al₂O₃ ethylene oxychlorination catalysts, J. Catal. 179 (1998) 606–618.

[35] G. Leofanti, M. Padovan, M. Garilli, D. Carmello, A. Zecchina, G. Spoto, S. Bordiga, G.T. Palomino, C. Lamberti, Alumina-supported copper chloride: 1. Characterization of freshly prepared catalyst, J. Catal. 189 (2000) 91–104.

[36] E.W. McFarland, H. Metiu, Catalysis by doped oxides, Chem Rev 113 (2013) 4391–4427.

[37] Y. Hinuma, T. Toyao, T. Kamachi, Z. Maeno, S. Takakusagi, S. Furukawa, I. Takigawa, K.-I. Shimizu, Density functional theory calculations of oxygen vacancy formation and subsequent molecular adsorption on oxide surfaces, J. Phys. Chem. C 122 (2018) 29435–29444.

[38] G. Kumar, S.L.J. Lau, M.D. Krcha, M.J. Janik, Correlation of methane activation and oxide catalyst reducibility and its implications for oxidative coupling, ACS. Catal. 6 (2016) 1812–1821.

[39] Y. Qi, C. Aaserud, J. Yang, A. Holmen, D. Chen, Promotional effect of in-situ generated hydroxyl on olefin selectivity of Co-catalyzed Fischer-Tropsch synthesis, Phys. Chem. Chem. Phys. (2019).

[40] Y.-A. Zhu, D. Chen, X.-G. Zhou, W.-K. Yuan, DFT studies of dry reforming of methane on Ni catalyst, Catal. Today. 148 (2009) 260–267.